Published online 15 July 2008

Nucleic Acids Research, 2008, Vol. 36, No. 15 ***e98***
doi:10.1093/nar/gkn436

Electrical detection of the temperature induced melting transition of a DNA hairpin covalently attached to gold interdigitated microelectrodes

Greg P. Brewood[1,*], Yaswanth Rangineni[2], Daniel J. Fish[1], Ashwini S. Bhandiwad[1], David R. Evans[3], Raj Solanki[2,4] and Albert S. Benight[1,4,5]

[1]Portland Bioscience, Inc., Portland, OR 97201, [2]Department of Electrical & Computer Engineering, Portland State University, [3]SHARP Laboratories of America, Inc., Camas, WA 98607, [4]Department of Physics and [5]Department of Chemistry, Portland State University, Portland, OR 97207, USA

Received October 10, 2007; Revised and Accepted June 24, 2008

ABSTRACT

The temperature induced melting transition of a self-complementary DNA strand covalently attached at the 5′ end to the surface of a gold interdigitated microelectrode (GIME) was monitored in a novel, label-free, manner. The structural state of the hairpin was assessed by measuring four different electronic properties of the GIME (capacitance, impedance, dissipation factor and phase angle) as a function of temperature from 25°C to 80°C. Consistent changes in all four electronic properties of the GIME were observed over this temperature range, and attributed to the transition of the attached single-stranded DNA (ssDNA) from an intramolecular, folded hairpin structure to a melted ssDNA. The melting curve of the self-complementary single strand was also measured in solution using differential scanning calorimetry (DSC) and UV absorbance spectroscopy. Temperature dependent electronic measurements on the surface and absorbance versus temperature values measured in solution experiments were analyzed assuming a two-state process. The model analysis provided estimates of the thermodynamic transition parameters of the hairpin on the surface. Two-state analyses of optical melting data and DSC measurements provided evaluations of the thermodynamic transition parameters of the hairpin in solution. Comparison of surface and solution measurements provided quantitative evaluation of the effect of the surface on the thermodynamics of the melting transition of the DNA hairpin.

INTRODUCTION

There is a substantial demand for analytical platforms capable of detecting specific DNA sequence markers. Structural transitions associated with specific nucleic acid interactions often serve as the central feature for sensing external samples. However, prior to building a sensor to detect external samples, inherent features of the sensing element on the specific detection platform must be calibrated. That is, when DNA transitions comprise the sensing element, selected sequences can be designed to provide molecular transitions with specifically desired features. Evaluation of thermodynamic parameters and melting properties of the DNA on the surface where the reaction takes place is required for optimal design of sensing elements.

In contrast to the same hybridization reactions that occur on the surface, reactions of DNA in solution are easier to characterize. Thermodynamic parameters of these reactions can be evaluated directly from solution measurements and employed to calibrate signals measured by the sensor for the same reactions on the surface. A standard measure of the solution thermodynamic stability of short duplex DNAs is the melting temperature, T_m. Melting temperature is defined to be the point where half of the DNA exists in the duplex state and half exists as single strands. Solution T_ms are used both to design and characterize DNAs in hybridization reactions. Under comparable conditions, when one strand of the duplex is attached to a surface, T_m is reportedly different ($>10°C$ in some cases) than for the same duplex DNA in solution (1,2). Although this effect on T_m crudely reflects the influence of the surface on the stability of the duplex, it provides little insight into how thermodynamics of the hybridization reaction are affected by the surface.

*To whom correspondence should be addressed. Tel: +503 725 2350; Fax: +503 725 2305; Email: gbrewood@pdxbio.com

General models of nucleic acid helical stability have been deduced that are applicable to estimate thermodynamic parameters of short duplex DNAs with well defined sequences. These approaches rely on established sets of nearest-neighbor (n-n) stability parameters evaluated from solution melting experiments (3,4). Employing these parameters for stability calculations of short duplex DNAs in solution is standard practice and in most cases, predictions provide reasonable agreement with experimental results in solution (3–13). Stabilities are often calculated using the n-n solution parameters. An implicit assumption underlying the use of the n-n model to predict extents of hybridization on different sensing platforms is that the thermodynamic rules governing strand annealing remain the same in the vicinity of the surface (if even in a relative sense), compared with in solution. Even so, different surfaces are likely to contribute to the overall stabilities of reaction products in different ways. For different sensing platforms, effects of the surface on molecular properties and interaction chemistries just above the surface are expected to be inherently complex in nature.

In this study, a DNA oligonucleotide was designed with complementary sequences on each end so as to promote formation of a stable intramolecular structure, with 20 bp in the stem and a four base loop, at temperatures below the melting temperature. The DNA was synthesized with a 5′-C_6-thiol linker for attachment to the surface of gold interdigitated microelectrodes (GIME). The temperature induced melting transition from the surface-attached hairpin structure to the melted, single-stranded species was then detected using impedance spectroscopy.

The solution stability of the hairpin was determined by differential scanning calorimetry (DSC) and UV absorbance spectroscopy in the same buffer as in the surface-based electronic measurements. Thermodynamic parameters derived from solution measurements were used to generate theoretical two-state model curves fit to the impedance spectroscopy transition data. Comparison of the curves derived from the two measurements indicated the hairpin to be more stable on the surface.

Figure 1. DNA hairpin melting reactions (**A**) DNA hairpin (containing 5′ C_6-thiol linker) in solution melts to a single strand. The temperature induced melting transition of the hairpin in solution was studied by DSC and UV absorbance versus temperature measurements. (**B**) DNA hairpin attached at the 5′ end to gold electrodes via a C_6-thiol linker. The temperature induced melting transition hairpin on the surface was monitored by measuring four distinct electronic properties of the molecule; Z, θ, C and D, over a 10^6 frequency range at different temperatures.

MATERIALS AND METHODS

DNA

The synthetically prepared single-stranded DNA (ssDNA) oligonucleotide was purchased from Integrated DNA Technologies (Coralville, IA). As shown in Figure 1, the 44 base sequence was designed to form a stable intramolecular hairpin structure (the hairpin has 20 duplex base pairs in the stem and a four base single strand loop). The first 20 bases on the 5′ end are complementary to the last 20 bases on the 3′ end. DNAs were synthesized with a C_6-thiol modification on the 5′ end for attachment to gold surfaces and were ordered with standard purification. Since only full length synthetic strands contained the 5′ thiol modification, only full length strands were attached to the surface.

Attachment to gold surfaces

Single-stranded oligonucleotides were attached to gold electrode surfaces through the C_6-thiol linker modification on the 5′ end using reaction conditions taken from the literature (14–19). As recommended by the supplier (www.idtdna.com), DNA was stored in a buffered solution containing 10 mM dithiothreitol (DTT) and 1× TE (10 mM Tris, 1 mM EDTA) at pH = 7.4. DTT was used to chemically reduce the thiol-functional group and was removed by extracting the solution four times with ethyl acetate prior to attachment reactions of the thiolated-ssDNA to the gold electrodes. Final reaction conditions used for attachment contained 50 μM HS-ssDNA, 0.5× TE, 0.5 M KH_2PO_4, pH = 3.8. Reactions were incubated at room temperature for at least 16 h. To remove residual salt after completion of the process, chips were washed with ultra pure H_2O.

Reaction conditions

The buffer used for measurements of temperature induced transitions of DNAs attached to gold electrodes contained 0.1× TE (1 mM Tris, 0.1 mM EDTA at a pH of 7.4). The tris base was titrated using HCl, so the primary cation present in reactions is $Tris^+$. The primary anion is Cl^-. Because impedance spectroscopy (described below) was used to monitor the transition and since the technique is based on displacement of charges, a low salt buffer was required to minimize signals originating from salt ions. The same buffered solvent conditions (0.1× TE) were used for both surface and solution measurements. This provided more reliable comparisons between thermodynamic transition parameters determined in solution and on the surface. It is curious that in such a low salt environment the hairpin structure has any stability in solution or on the surface. On the surface, the local salt concentration in the neighborhood of the electrodes may be much

higher as electrodes could recruit counterions out of solution to the surface. This would result in a higher ionic strength in the local region of the electrode. However, the hairpin is apparently stable in solution under the same low salt conditions, which is also surprising.

Differential scanning calorimetry

Measurements of the excess heat capacity, ΔC_p, of DNA solutions as a function of temperature were made using a Nano-DSC™ (Calorimetry Sciences Corp., Lindon, UT). ΔC_p is the amount by which the apparent specific heat for a solution containing a solute exceeds the baseline specific heat of a solution with no added solute (20). A plot of ΔC_p versus temperature is the DSC melting curve. The transition temperature or T_m of a DSC melting curve is the temperature at which the maximum peak height is observed on the baseline-corrected ΔC_p versus temperature curve. The integrated area under the concentration corrected DSC melting curve provides the DSC transition enthalpy,

$$\Delta H_{cal} = \int \Delta C_p dT \quad \mathbf{1}$$

The DSC transition entropy values are determined from the integrated area under the plotted curve of $\Delta C_p/T$ versus temperature,

$$\Delta S_{cal} = \int \frac{\Delta C_p}{T} dT \quad \mathbf{2}$$

For DSC melting curves, DNA samples in 0.1× TE buffer were heated and cooled at a rate of 120°C/h over the temperature range from 15°C to 105°C. Two heating (melting) curves and two cooling curves were collected for every sample. Data were analyzed using the CpCalc™, version 2.1 software package from Applied Thermodynamics Corp., USA. The analysis yielded values of the enthalpy, ΔH_{cal}, and entropy, ΔS_{cal} for the melting transition. These evaluated parameters were used subsequently in two-state model analyses of the acquired data.

UV absorbance spectroscopy

Optical melting curves were collected as the absorbance at 268 nm versus temperature using a Hewlett-Packard™ 8452a diode array spectrophotometer with a 89090A Peltier™ temperature station. Absorbance values were measured at a heating rate of 120°C/h over the temperature range from 20°C to 100°C. Values of thermodynamic transition parameters were estimated from graphical analysis of the differential melting curves as previously reported (21). Reported parameters are average values obtained from multiple (at least two) independent melting experiments.

Gold interdigitated microelectrodes

Interdigitated electrodes are comprised of micrometer sized intertwined gold fingers that provide maximum interaction over a small area. A micrograph of a GIME is shown in Figure 2A. Each gold electrode 'finger' had dimensions (width × length × height) = 1 μm × 100 μm × 0.2 μm. The corresponding surface area provided a sufficiently large substrate for attachment of ssDNA. A schematic of a GIME cross-section depicting well dimensions, DNA attachment to their modified gold surfaces and the source of electrical measurements is shown in Figure 2B. Each chip had a total of 50 electrodes, 25 for each polarity and a gap spacing of 1 μm between each electrode. Small dimensions of the sensors allows for simultaneous probing of several sets of GIMEs leading to increases in sensitivity, higher signal-to-noise ratios and greater reliability of collected data. Quality and efficiency of collected electrical signals is influenced by electrode length, gap size and total number of electrodes.

Electrical measurements

Dielectric response of macromolecules placed in an external electrical potential can be measured using impedance spectroscopy. However, it is essential that the molecules be bound to the electrode surface so that polarization changes induced in the molecules can be detected. Molecules not bound to the surface, but suspended in buffer solution, are likely to undergo oscillations in response to the applied alternating electric field. This produces a broad signal devoid of specific molecular signatures. GIMEs were fabricated following standard processes commonly employed throughout the microelectronic industry. Electrodes were fabricated on top of a 100 nm thick layer of silicon oxide grown on silicon wafers. Measurements at elevated temperatures were difficult due to evaporation of the liquid sample during the course of temperature dependent experiments. To minimize evaporation, glass tubing cut in half along the longitudinal axis, was placed on top of the chip to produce a cavity sealed around the edges. A small hole at one end of this enclosure allowed the fluid in the cavity to expand and provided a port through which to add solutions to the cavity. For external connection, contact arms of the GIMEs protruded beyond the cavity.

Impedance measurements

Impedance spectroscopy generally involves small-signal measurement of the electrical response of a material of interest and subsequent analysis of the response to yield useful information regarding physicochemical properties of the system (22). An alternating electric field was utilized to probe electrical properties of the immobilized molecules and their interfaces with electrically conducting electrodes. Measurements were made using a circuit composed of GIMEs and an impedance meter (HP 4192A) while varying temperature and frequency of the applied alternating electric field. Impedance measurements were made on a probe station that was equipped with a sample holder that could be heated. For actual measurements, a chip was placed on the holder and the GIMEs were contacted at the protruding arms with fine wire tips. Initially, room temperature measurements were made and served as the base line. Subsequently, measurements of four electronic parameters over a wide frequency range (described below) were recorded at 30, 40, 50, 60, 70 and 80°C.

At each temperature the four electrical parameters, Z, θ, D and C were monitored over a frequency range from

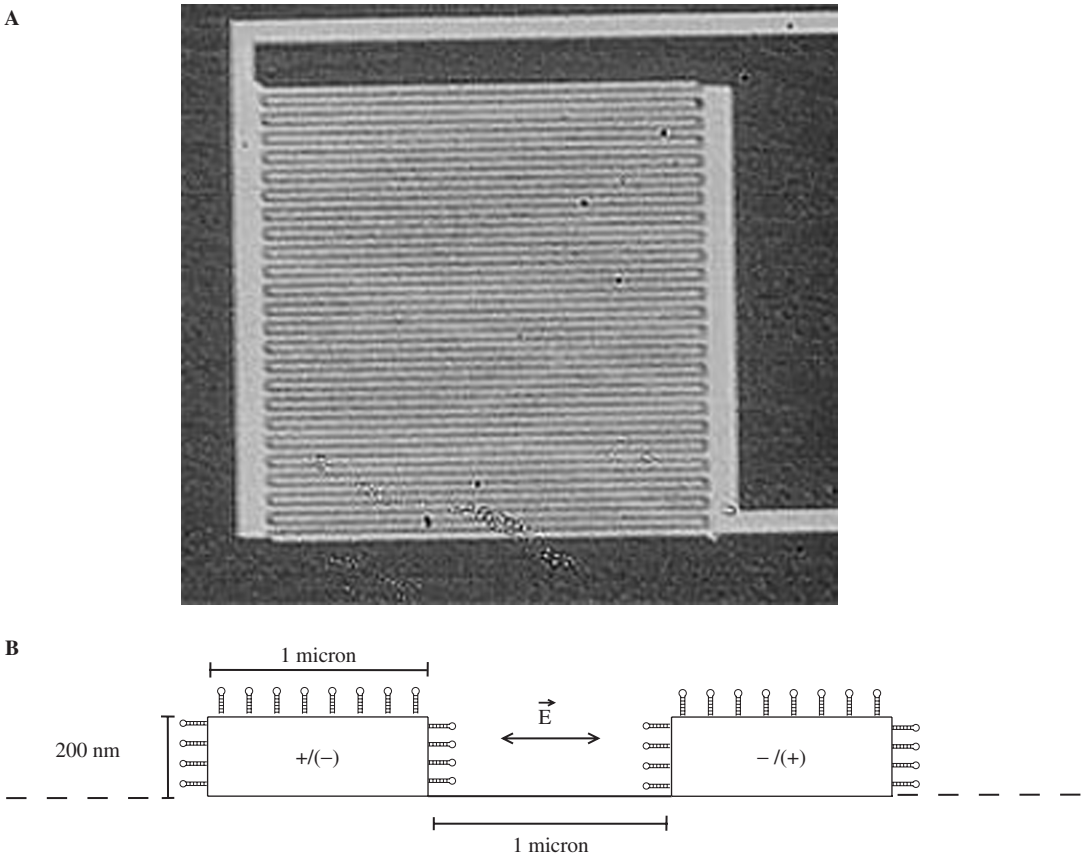

Figure 2. GIMEs (**A**) Micrograph image of an interdigitated electrode comprised of micron-sized intertwined metal fingers that allow a maximum interaction over a small area. Each chip had a total of 100 electrodes, 50 for each polarity, and a gap 'spacing' of 1 μm between the interdigitated electrodes. (**B**) Schematic cross-section of two interdigitated electrodes. The width of each 'finger' is 1 μm and the length is 100 μm. The heights of the electrodes are 200 nm and provided a large surface area for attachment of the ssDNA allowing enhanced sensitivity. DNAs attached to the surface are subjected to an alternating electric field, $\vec{E}$, and electrical measurements are measured.

5 Hz to 13 MHz. Impedance (Z) is the complex resistance, (i.e. resistance when the phase difference between the applied voltage and current is nonzero); Phase angle (θ) is the phase difference between the voltage and the current; dissipation factor (D) is the ratio between the complex resistance and resistance when the phase is zero; and capacitance (C) is the charge per unit voltage. To minimize contributions from buffer components and circuit parasitics, room temperature values for each of the four parameters were subtracted from corresponding values measured at different temperatures.

RESULTS

Solution measurements

Multiple temperature dependent measurements of the behavior of DNA samples were acquired using two different techniques. Both optical absorbance spectroscopy and DSC are consistent with the DNA forming a hairpin in solution. Subsequent to solution measurements, the DNA sample was diluted and the electrical conductivity of the solution measured to confirm the salt concentration (data not shown). Conductivity measurements were entirely consistent with the extremely low salt condition (1 mM Tris). It is quite remarkable that intramolecular hairpins could form under these conditions.

Optical melting curves

A plot of the absorbance measured at 268 nm versus temperature for the self-complementary single strand in 0.1× TE buffered solvent is shown in Figure 3A. Optical melting curves exhibited sigmoidal transitions with distinct lower linear base lines, attributed to the duplex hairpin and upper linear base lines corresponding to melted single strands. The normalized optical melting curve, representing the fraction of melted hairpin (α) versus temperature, is shown in Figure 3B. The derivative curve, $d\alpha/dT$ versus temperature, is shown in Figure 3C (dash–dot line). The temperature at the maximum peak height of the derivative curve is the melting temperature, T_m. Thermodynamic parameters for the melting transition were evaluated by graphical analysis of the derivative curve in Figure 3c using Equation (S9) of the Supplementary Material. Values of graphically evaluated thermodynamic parameters are given in Table 1.

Thermodynamic transition parameters estimated from graphical analysis of optical melting implicitly assume the hairpin melting process is two-state, i.e. there are no

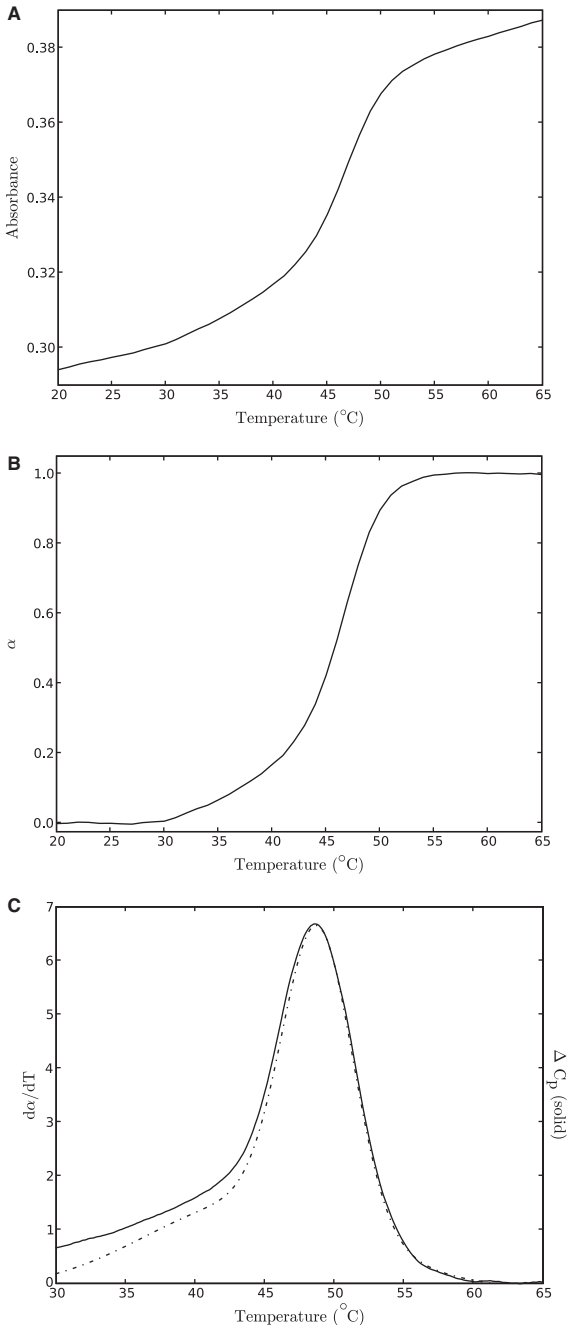

Figure 3. Melting curves. (**A**) Raw absorbance measured at 268 nm as a function of temperature for the hairpin molecule in Figure 1A. Data were collected for one cooling cycle and two separate heating cycles and averaged. Measurements were made over a temperature range from 20°C to 100°C at a heating rate of 120°C/h. (**B**) Fraction of broken base pairs α (T) versus temperature obtained from the raw absorbances versus temperature in (A). This curve was obtained by normalizing the fractional absorbance change versus temperature between lower and upper linear baselines (23). (**C**) Comparison of the optical and DSC melting curves. The plot of the fraction of broken base pairs (α) versus temperature curve was smoothed by fitting a sigmoidal curve to the data in (B) and the smooth derivative plot of $d\alpha/dT$ versus temperature was obtained (dash–dot line). The DSC melting curve of the excess molar heat capacity, ΔCp versus temperature (solid line) is also shown for comparison. Integration of this curve gives a direct measurement of the heat involved in the melting transition. The curve shown is an average of four different scans; two from heating and two cooling cycles. The T_m values are slightly different but the curve shapes are similar.

Table 1. Thermodynamic transition parameters measured by DSC and graphically estimated from A_{268} versus temperature measurements in a buffered 0.1× TE solution

	ΔH° (kcal/mol)	ΔS° (cal/Kmol)	ΔG°(25°C) (kcal/mol)	T_m (°C)
DSC	72.0 ± 1.9	224 ± 6	5.3 ± 2.6	48.6 ± 0.8
UV Absorbance	73.3 ± 0.8	229 ± 2	5.1 ± 1.0	47.0 ± 0.1

Evaluated solution parameters (ΔG° values) were used to fit the two-state model to the melting transition of the DNA hairpin attached to the gold surface and monitored by impedance spectroscopy.

partially melted intermediate states. Consequently, derived parameters are inherently model-dependent. Accuracy of the two-state model and thermodynamic parameters evaluated from analysis of optical melting curves can be quantitatively ascertained by comparison with values measured by DSC.

DSC melting curves

DSC measurements provide measures of the excess heat capacity changes during the temperature induced melting reaction and thereby provide direct measurements of transition thermodynamic parameters. DSC thermodynamic parameters are model-independent, therefore. A plot of the excess heat capacity, ΔC_p, versus temperature obtained by DSC is co-plotted in Figure 3C for comparison (solid line). To compare the optical and DSC shapes, the derivative melting curve obtained from optical measurements (and displayed in Figure 3C) was scaled and shifted to align with the DSC T_m. The two curves are quite comparable and thermodynamic parameters evaluated by DSC and optical melting are listed in Table 1. There is a slightly more prominent shoulder on the DSC curve. As expected for a hairpin melting transition, T_m values measured by both techniques are equivalent within experimental error. However, thermodynamic parameters extracted from both types of melting curve measurements were lower than anticipated for the presumed hairpin structure. The greatly decreased thermodynamic stability in the low salt environment might be expected.

An alternate explanation for the observed smaller than expected enthalpy of melting is that the hairpin has degraded. Although an obvious possibility, we consider it quite remote for the following reasons. Multiple surface and solution experiments (at least four replicates) were conducted. All gave consistent results and throughout no evidence of degradation was observed whatsoever. In such a low Na^+ environment, it would be expected that significantly lower values of the thermodynamic parameters might be obtained due to a lower stability. However, it is quite remarkable that intramolecular hairpins actually form under these conditions.

Comparisons of parameter values in Table 1 reveal the optical values of ΔH° and ΔS° are in agreement with those obtained from DSC measurements. It should be noted the choice of baselines has a significant effect on the value of the peak height on the derivative melting curve, from which ΔH° is examined. Likewise, parameters

obtained from DSC measurements are dependent upon the pre- and post-transition baselines. Therefore, it is essential that baseline regions from both optical and DSC techniques be consistently analyzed. The thermodynamic parameters combined with the comparable T_m values measured by optical and DSC melting indicates essentially the same reaction was monitored by both techniques. Agreement between the experimental T_m and thermodynamic parameters obtained from the model-dependent (optical melting) analysis and directly measured by DSC are not inconsistent with the two-state assumption. The data are rather high quality in that the relative errors of measured thermodynamic parameters evaluated by DSC or UV absorbance are <3%.

Directly measured thermodynamic parameters evaluated in solution using DSC (and given in Table 1) were used in a two-state fit of the model to the melting transitions measured electronically on the surface. In analysis of both solution and surface melting data it is assumed only two molecular states occur throughout the transition (i.e. the duplex hairpin and melted single strands). Contributions of partially melted intermediates to the melting process and melting curve shape are presumed to be minimal. Validity of this assumption was obtained from results of both solution and surface melting measurements that showed quite comparable qualitative behavior. Quantitative differences were presumably due to a combination of surface effects and temperature dependent features of the particular electrical signals used to monitor the hairpin melting transition.

Melting curves on GIMEs

The hairpin to single strand melting transition of the surface-attached DNA was monitored electronically as a function of temperature. Measurements were collected on eight different GIME devices and produced entirely consistent results. Temperature was varied from 30°C to 80°C while distinct (albeit different) changes in Z, θ, D and C were observed. Changes in each electrical parameter were monitored, at distinct frequencies displaying the largest changes, to produce the temperature profiles shown in Figure 5. Melting transitions were consistent with a two-state model. Typical frequency scans of the four electrical parameters, Z, θ, D and C, at six different temperatures averaged over similar data collected on eight different devices are shown in Figure 4.

Analysis and comparison of solution and surface melting transitions

Each electrical signal measured as a function of temperature displayed a consistent trend. At temperatures below T_m, average measured intensities were essentially constant and distinct from signal intensities measured above T_m that were clearly at a different average intensity. Electrical melting curves were analyzed assuming that the temperature dependent molecular process on the surface occurs in a two-state manner.

For reactions in solution, derivation of equilibrium properties associated with hairpin melting transitions have been described previously (5,23). The same analysis is extended here to include effects of the surface in the unimolecular hairpin melting reaction. The thermodynamic stability of a DNA hairpin reaction constrained to a surface is assumed here to consist of three distinct and separate components; the Stem, Loop and Surface as shown in Equation (3). Details of the model analysis are provided in the Supplementary Material. The total free energy of the hairpin melting reaction is given by,

$$\begin{aligned}\Delta G_{total} &= \Delta G_{stem} + \Delta G_{loop} + \Delta G_{surface} \\ &= \Delta G_{soln} + \Delta G_{surface}\end{aligned} \quad \mathbf{3}$$

ΔG_{stem} is the free energy that arises from formation of the duplex stem, ΔG_{loop} is the free energy due to formation of the loop and $\Delta G_{surface}$ is a term that arises from interactions of the hairpin molecule with the surface. For a hairpin in solution, ΔG_{stem} and ΔG_{loop} are combined into a single term denoted ΔG_{soln} that represents the stability of the hairpin in the solution environment. ΔG_{soln} values were calculated from thermodynamic enthalpy and entropy parameters measured in solution experiments.

Experimentally measured melting curves, or plots of the fraction of observed signal change, α, versus temperature, were fit using a two-state model as described in the Supplementary Material (Equation S13) and used herein.

$$\alpha = \frac{K^{tot}}{1 + K^{tot}} = \frac{AK^{soln}}{1 + AK^{soln}} \quad \mathbf{4}$$

where K^{tot} is defined to be the equilibrium constant for reactions occurring on the surface. The equilibrium constant can be written as the product of two terms as

$$\begin{aligned}K^{tot} &= e^{(-\Delta G^{tot}/RT)} \\ &= e^{(-\Delta G^{surface}/RT)} \cdot e^{(-\Delta G^{soln}/RT)}\end{aligned} \quad \mathbf{5}$$

The single fitting parameter, $A = e^{(-\Delta G^{surface}/RT)}$, is considered to be a correction factor for effects due to the surface compared with melting in solution. Using a standard bounded minimization protocol [Jones, Eric, Oliphant, Travis and Pearu Peterson. (2001–) SciPy: Open source scientific tools for Python (www.scipy.org)], optimized fits yielded values of A.

Thermodynamic parameters, ΔH_{cal} and ΔS_{cal} determined by DSC melting curve analysis in the same buffered solution, were used in the fitting procedure. In this approach, melting transitions for the hairpins measured on the surface were fit with the two-state model by varying parameter A, from which the value of K^{tot} was determined according to Equation (5). Extracted values of A that produced the best fits to the data, are summarized in Table 2 and the fits produced are shown as solid black lines in Figure 5.

The value of A includes surface contributions to the hairpin melting reaction as measured by a specific electric parameter. Although A is expected to depend on a number of yet poorly understood factors, reported measurements indicate that the electrical properties provide a monitor of the same melting transition that occurs in solution, with added effects of the surface. These effects on different electric parameters can be quantitatively assessed through the values of A.

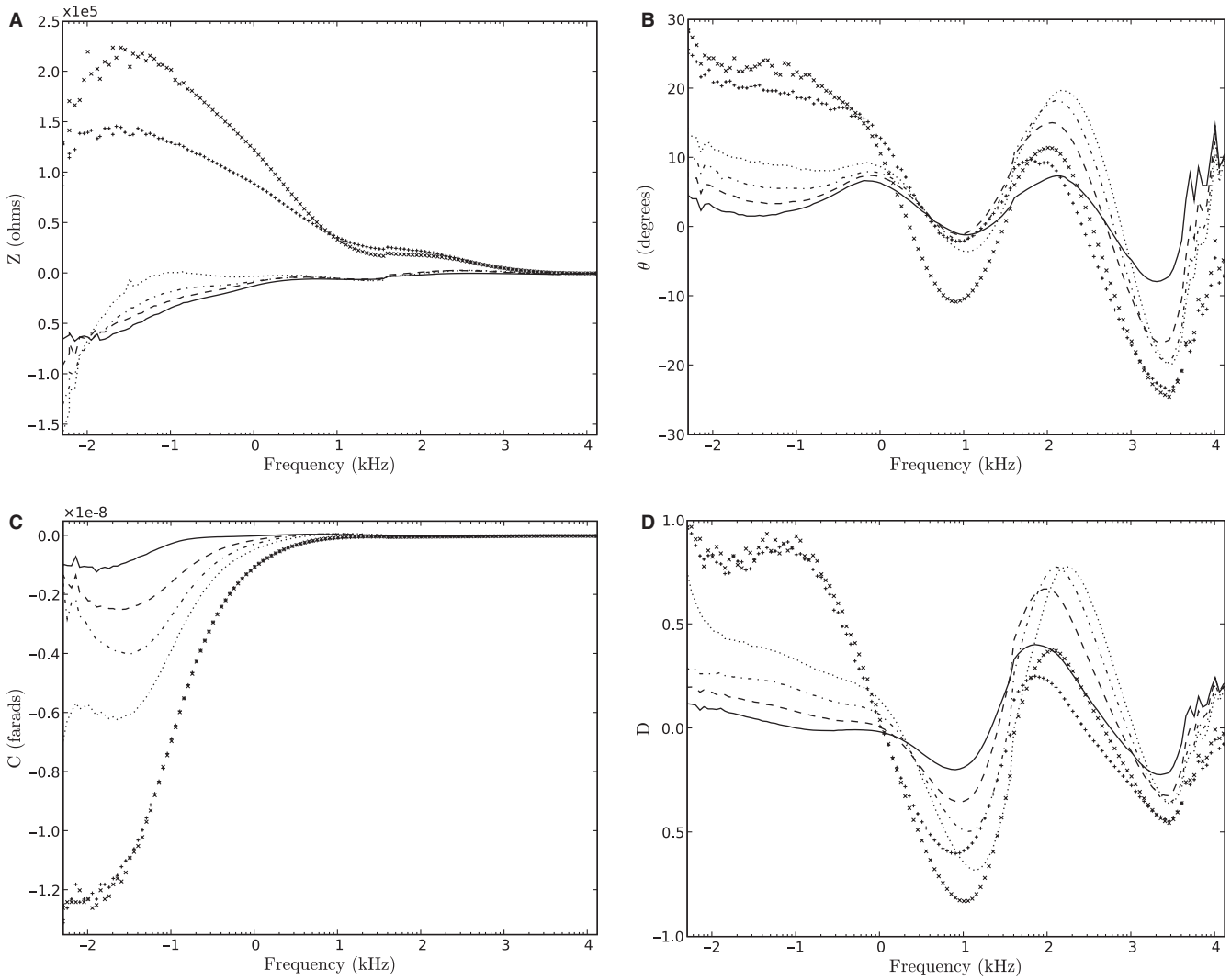

Figure 4. Electronic measurements as a function of frequency. Impedance measurements were made on a probe station equipped with a sample holder capable of heating the sample. For each electronic property, measurements at room temperature (20°C) served as base lines that were subtracted from each of the four parameters to remove the contributions from the buffer and circuit parasitics. Four electronic properties were recorded as a function of frequency at 30 (solid line), 40 (dash line), 50 (dash–dot line), 60 (dotted line), 70 (+) and 80 (×)°C. Typical frequency scans for four parameters are shown. The electronic parameters are: (**A**) Conductance/impedance versus frequency. (**B**) Phase Angle (θ) versus frequency. (**C**) Capacitance (*C*) versus frequency. (**D**) Dissipation factor (*D*) versus frequency.

All four electrical parameters show similar trends in the acquired data that indicate a distinct change in physical states can be detected electronically using GIME sensors. A fit of the simple two-state model to the data while employing the thermodynamic parameters measured in solution produces a curve that was used to calculate T_m. For hairpins attached to GIMEs, a $T_m = 62.0 \pm 3.2$°C is reported. In contrast, the same hairpin in solution has a $T_m = 47.8 \pm 0.4$°C (Table 1). The surface apparently stabilizes the duplex. Standard secondary structure prediction programs {Mfold [www.idtdna.com, (24)], DINAMelt (25) and AutoDimer (26)} predicted the hairpin to melt at temperatures above 40°C, even at low ionic strength (data not shown), consistent with observations.

In Figure 6, it is clear that attachment of the hairpin to the surface has a significant stabilizing effect, although sources of this stabilization are not currently understood. Two melting curves were measured for the hairpin.

Table 2. Surface correction evaluated from minimizing fits of the thermodynamic two-state model to the average melting data measured on the gold microelectrode surface (Figure 5)

	A	$\Delta G_{surface}$(25°C) (kcal/mol)
Z	0.0025 ± 0.0015	3.6 ± 0.4
θ	0.0091 ± 0.0080	2.8 ± 0.5
C	0.015 ± 0.0098	2.5 ± 0.4
D	0.042 ± 0.0096	1.9 ± 0.1
		$\overline{\Delta G}_{surface} = 2.7 \pm 0.2$

The melting curve shown by a solid black line is a fit of the normalized, average electronic data for the hairpin reaction occurring on the surface (shown in Figure 5E). The melting curve of the hairpin in solution is shown by a black dot–dash line. Differences between these curves

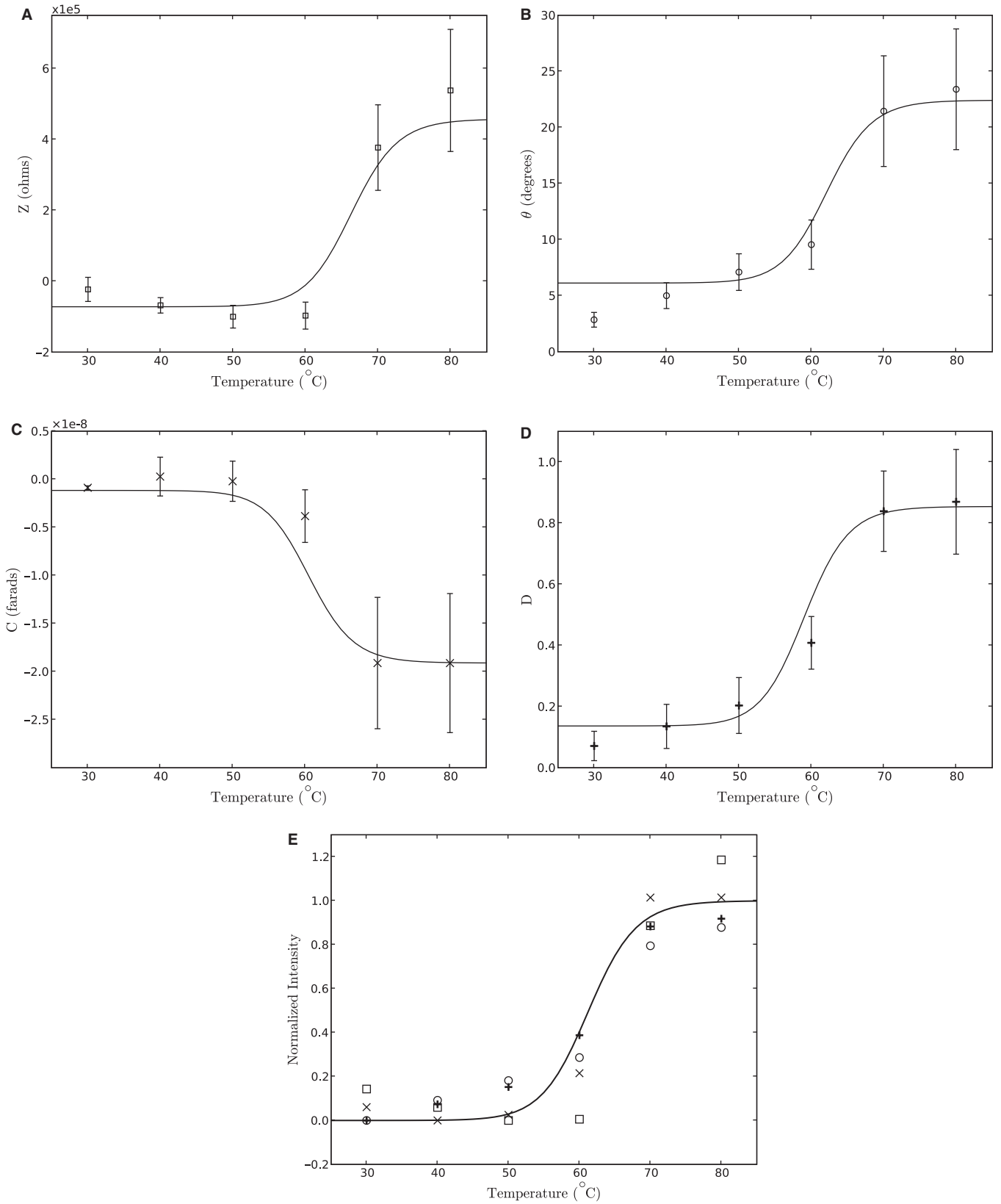

Figure 5. Electronic measurements as a function of temperature at a single frequency for each of the four parameters. Presented data were collected on eight different devices and error bars are the standard deviations from multiple measurements. Also shown are the best fit lines generated by Equation (4) (see text). (**A**) Impedance versus temperature. (**B**) Phase angle versus temperature. (**C**) Capacitance versus temperature. (**D**) Dissipation factor versus temperature. (**E**) Data points shown in (A–D) were normalized to their individual transition plateaus and co-plotted. The best fit line (solid black) was generated by fitting Equation (4) to the average data. Open squares and circles signify the normalized intensities.

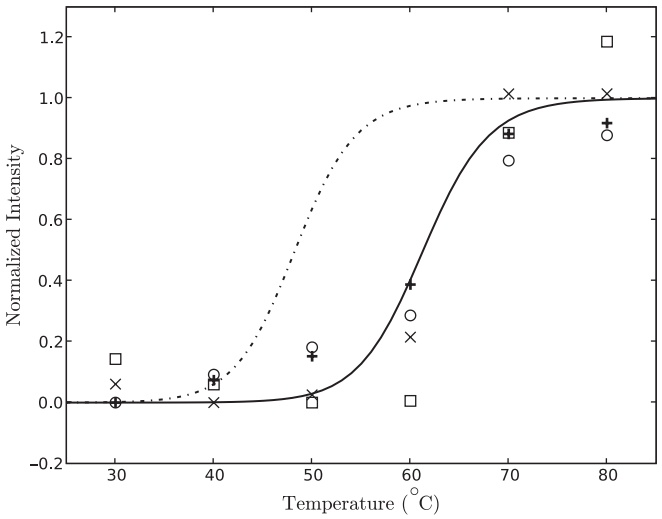

Figure 6. Comparison of solution and surface melting curves. The melting curve for the hairpin attached to the surface shown in Figure 5E is shown by a solid line. The dash–dot line is the melting curve for the same hairpin in solution generated from measured thermodynamic transition parameters evaluated in DSC measurements and assuming a two state transition. The significant difference in the T_m values is attributed to effects of the surface on the hairpin melting transition.

determined by the melting temperatures clearly indicate that the GIME has a stabilizing effect on the hairpin melting transition. Although origins of stabilization arising from attachment of the hairpin DNA to the gold surface are unknown, the observed increase in stability is consistent with reported observations of increased stabilities for DNA hybridization reactions occurring on surfaces. Higher melting temperatures were reported for a short DNA duplex formed with one strand attached to a surface compared with the same duplex in solution. This indicated stabilization of the duplex on the surface (1). Halperin *et al*. (27) developed a model that assumed the surface to be an impenetrable wall, thereby reducing the number of configurations available to a terminally anchored ssDNA. Increased stability was attributed to a reduction in the configurational entropy of the surface attached DNA hybridization products. This explanation is entirely consistent with our observations but many details remain elusive and a more thorough characterization of such surface reactions, including specific effects of the surface charge should be performed.

DISCUSSION

Results demonstrated that intramolecular structural transitions of hairpins attached to GIMEs can be measured electronically using impedance spectroscopy. Addition of a C_6-thiol group to the end of the single strand for attachment of the DNA oligonucleotide to the surface is the only modification required. Experimental measurements detected a change in four different electrical parameters as a function of temperature. Because measured transitions for each electrical property occurred at nearly identical temperatures, detected signal changes were attributed to melting of the DNA hairpins.

Presumably the GIMEs are sensitive to differences in charge densities near the surface and as such, can detect physical changes in structure between the duplex hairpin and single strand states of a DNA strand. The phosphate backbone of DNA is negatively charged so the hybridization event (formation of the duplex stem of the hairpin) could dramatically increase the charge density near the surface. The distance over which this effect extends is unknown. Conceivably, electrodes could be tuned to optimize a clear difference in measured signal between a duplex hairpin and a fully extended bimolecular duplex that can form between the single strand on the surface and a second complementary single strand in solution.

Analytical characterizations arising from measurements by impedance spectroscopy involve detection of net displacements of charged species in a solution to which the electrode is in contact. As such, a low salt buffer was required to minimize the signal originating from salt ions. In this regard, detected signals were isolated on individual DNA polyions in the same solution. It is essential that the molecules be bound to the electrode surface so that polarization changes induced in the molecules can be detected. Molecules (of all types) not bound to the surface, but suspended in buffer solution, also undergo oscillations in response to the applied alternating electric field. However, this produces a broad signal devoid of specific molecular signatures.

In the analytical approach employed herein, potential effects of the surface on thermodynamic stabilities of reaction products are investigated. Effects are characterized by a single thermodynamic term, or correction factor (shown in Table 2). This factor, in turn, can be used to independently predict stabilities of reaction products on a particular surface based on the solution thermodynamic characteristics of the reactants and products formed. Conversely, perturbations from solution stabilities caused by surface effects can be utilized to calibrate biosensor output. If reaction thermodynamics are well characterized in solution, observed differences on the surface from solution behavior can be attributed to 'surface specific' effects on the sensing reaction inherent to any particular platform. Assuming effects of the surface can be considered independent and separable, the total thermodynamic stability on the surface can be partitioned into 'surface dependent' and 'surface independent' parts, the latter being the solution values of experiments. This approach provides a foundation for inter-comparison of acquired signals from different platforms that may have distinctly different surface features. Although it is expected that effects of interactions between surfaces and reactions occurring just above the surfaces are complex in nature, it is assumed herein that the two components are separable only as a first approximation. Physical properties and fine features specific to individual surface potentials is a more challenging problem that will not be addressed.

Diagnostic detection using probes that form hairpins has been employed to detect single-stranded DNA targets in solution (17,28). The hybridization process in this context is indirectly detected through a physical change in the structure of the hairpin that allows hybridization of the

target to the probe. Such strategies provide the impetus to further develop the electrical technique into a biosensor based on detection of the bifunctional structural transitions in DNA hairpins. Similar strategies have been implemented in a number of DNA detection technologies. For example, molecular beacons use ssDNAs that form hairpins that can be detected optically because the DNA has a fluorophore on one end that is quenched by a fluorescence quencher on the other end when the ssDNA is in the hairpin conformation (28). Molecular beacon probes are designed with loops that contain significant portions complementary to the targets in solution. When no target complementary to the hairpin probe is present in solution, the ssDNA probe remains in the duplex hairpin state that puts the quencher molecule in the immediate vicinity of the fluorophore and thereby quenches the fluorescence resulting in relatively low intensity signals. When targets complementary to the probe are present in solution, hybridization will occur between the probes and complementary targets that are thermodynamically more stable than the hairpin species. In this conformation, the quencher and fluorescent molecules are far apart from each other so very little quenching of the signal occurs. Probes in this conformation generate much higher intensity signals.

In order for hairpin probes coupled to GIMEs to serve as effective electronic biosensors, successful discrimination between a full length, perfectly matched duplex and the (smaller) duplex hairpin attached to the surface must be demonstrated. In solution conditions, targets that are perfectly complementary to the hairpin are more stable than the hairpin itself and compete for reaction sites on the hairpin sequence. Understanding how the surface term affects the same competition reaction between perfect match probe-target pairs and duplex hairpins on the surface is an important step towards validation of the GIME platform. Sequence dependent thermodynamics dictates that the fully complementary sequence will have a higher stability than the hairpin even in the presence of the surface. Differential detection of each duplex species using GIME and impedance spectroscopy are underway to demonstrate that this platform can efficiently detect each species in solution and can provide reliable characterization via differences between the two signals. That the different electrical signals provide somewhat unique temperature dependent signatures makes it attractive to explore the extent to which these distinct changes are related to different physical characteristics of the structural changes that accompany the melting transition. Interpretations of the electrical measurements on this level may be difficult to actually achieve, but are at least conceivable from these measurements.

It remains to be shown that electrical measurements can be employed in place of fluorescence detection to discern between a single strand in a duplex hairpin, intramolecular structure and the same strand in a longer duplex structure with a second complementary single strand. If this can be demonstrated, GIMEs may constitute an alternative label free sensing platform for DNA hybridization.

SUPPLEMENTARY DATA

Supplementary Data are available at NAR Online.

ACKNOWLEDGEMENTS

We thank the reviewers for instructional comments. We also gratefully acknowledge Dr Jim Goodarzi for careful reading of the manuscript and useful suggestions and Saba Alemayehu for expert technical assistance. Funding to pay the Open Access publication charges for this article was provided by Portland Bioscience Inc.

Conflict of interest statement. None declared.

REFERENCES

1. Finot,E., Bourillot,E., Meunier-Prest,R., Lacroute,Y., Legay,G., Cherkaoui-Malki,M., Latruffe,N., Siri,O., Braunstein,P. and Dereux,A. (2003) Performance of interdigitated nanoelectrodes for electrochemical DNA biosensor. *Ultramicroscopy*, **97**, 441–449.
2. Meunier-Prest,R., Raveau,S., Finot,E., Legay,G., Cherkaoui-Malki,M. and Latruffe,N. (2003) Direct measurement of the melting temperature of supported DNA by electrochemical method. *Nucleic Acids Res.*, **31**, e150.
3. SantaLucia,J. Jr. (1998) A unified view of polymer, dumbbell, and oligonucleotide DNA nearest-neighbor thermodynamics. *Proc. Natl Acad. Sci. USA*, **95**, 1460–1465.
4. SantaLucia,J. Jr and Hicks,D. (2004) The thermodynamics of DNA structural motifs. *Annu. Rev. Biophys. Biomol. Struct.*, **33**, 415–440.
5. Breslauer,K.J. (1994) Extracting thermodynamic data from equilibrium melting curves for oligonucleotide order-disorder transitions. *Methods Mol. Biol.*, **26**, 347–372.
6. Breslauer,K.J., Frank,R., Blocker,H. and Marky,L.A. (1986) Predicting DNA duplex stability from the base sequence. *Proc. Natl Acad. Sci. USA*, **83**, 3746–3750.
7. Hall,T.S., Pancoska,P., Riccelli,P.V., Mandell,K. and Benight,A.S. (2001) Sequence context and thermodynamic stability of a single basepair mismatch in short deoxyoligonucleotide duplexes. *J. Am. Chem. Soc.*, **123**, 11811–11812.
8. Hillen,W., Goodman,T.C., Benight,A.S., Wartell,R.M. and Wells,R.D. (1981) High resolution experimental and theoretical thermal denaturation studies on small overlapping restriction fragments containing the *Escherichia coli* lactose genetic control region. *J. Biol. Chem.*, **256**, 2762–2766.
9. Marky,L.A. and Breslauer,K.J. (1982) Calorimetric determination of base-stacking enthalpies in double-helical DNA molecules. *Biopolymers*, **21**, 2185–2194.
10. Marky,L.A. and Breslauer,K.J. (1987) Calculating thermodynamic data for transitions of any molecularity from equilibrium melting curves. *Biopolymers*, **26**, 1601–1620.
11. Owczarzy,R., Vallone,P.M., Gallo,F.J., Paner,T.M., Lane,M.J. and Benight,A.S. (1997) Predicting sequence-dependent melting stability of short duplex DNA oligomers. *Biopolymers*, **44**, 217–239.
12. Wartell,R.M. and Benight,A.S. (1985) Thermal denaturation of DNA molecules: a comparison of theory with experiment. *Phys. Rep.*, **126**, 67–107.
13. Dimitrov,R. and Zuker,M. (2004) Prediction of hybridization and melting for double-stranded nucleic acids. *Biophys. J.*, **87**, 215–226.
14. Herne,T.M. and Tarlov,M.J. (1997) Characterization of DNA Probes Immobilized on Gold Surfaces. *J. Am. Chem. Soc.*, **119**, 8916–8920.
15. Yang,M., McGovern,M.E. and Thompson,M. (1997) Genosensor technology and the detection of interfacial nucleic acid chemistry. *Analytica Chimica Acta*, **346**, 259–275.
16. de-los-Santos-Álvarez,P.M., Jesus Lobo-Castanon,M., Miranda-Ordieres,A.J. and Tunon-Blanco,P. (2004) Current strategies for electrochemical detection of DNA with solid electrodes. *Anal. Bioanal. Chem.*, **378**, 104–118.
17. Fan,C., Plaxco,K.W. and Heeger,A.J. (2003) Electrochemical interrogation of conformational changes as a reagentless method for

the sequence-specific detection of DNA. *Proc. Natl Acad. Sci. USA*, **100**, 9135–9137.
18. Pividori,M.I., Merkoçi,A. and Alegret,S. (2000) Electrochemical genosensor design: immobilisation of oliognucleotides onto transducer surfaces and detection methods. *Biosens. Bioelectron.*, **15**, 291–303.
19. Wang,J. (2002) Electrochemical nucleic acid biosensors. *Anal. Chim. Acta.*, **469**, 63–71.
20. Sturtevant,J.M. (1987) Biochemical applications of differential scanning calorimetry. *Ann. Rev. Phys. Chem.*, **38**, 463–488.
21. Vallone,P.M., Paner,T.M., Hilario,J., Lane,M.J., Faldasz,B.D. and Benight,A.S. (1999) Melting studies of short DNA hairpins: influence of loop sequence and adjoining base pair identity on hairpin thermodynamic stability. *Biopolymers*, **50**, 425–442.
22. Macdonald,J.R. (1992) Impedance Spectrscopy. *Ann. Biomed. Eng.*, **20**, 289–305.
23. Owczarzy,R. (1999) Predictions of short DNA duplex thermodynamics and evaluation of next nearest neighbor interactions. *Ph.D. Thesis*. University of Illinois at Chicago, Chicago.
24. Zuker,M. (2003) Mfold web server for nucleic acid folding and hybridization prediction. *Nucleic Acids Res.*, **31**, 3406–3415.
25. Markham,N.R. and Zuker,M. (2005) DINAMelt web server for nucleic acid melting prediction. *Nucleic Acids Res.*, **33**, W577–W581.
26. Vallone,P.M. and Butler,J.M. (2004) AutoDimer: a screening tool for primer-dimer and hairpin structures. *BioTechniques*, **37**, 226–231.
27. Halperin,A., Buhot,A. and Zhulina,E.B. (2006) On the hybridization isotherms of DNA microarrays: the Langmuir model and its extensions. *J. Phys.: CondensMatter*, **18**, S463–S490.
28. Tyagi,S. and Kramer,F.R. (1996) Molecular beacons: probes that fluoresce upon hybridization. *Nat. Biotechnol.*, **14**, 303–308.